Effect of Stretching on the Precipitation Kinetics of an Al-2.0Li-2.8Cu-0.5Mg(-0.13Zr) Alloy

J.-D. KIM and J.K. PARK

The influence of stretching on the precipitation kinetics of an Al-2.0Li-2.8Cu-0.5Mg(-0.13Zr) alloy has been quantitatively investigated using transmission electron microscopy (TEM) and hardness testing. The microstructure of the alloy consists primarily of δ', S', and T_1 phases. Stretching exerts little influence on the coarsening kinetics of δ' phase. The activation energy for coarsening is estimated to be ~100 kJ/mole, regardless of whether the alloy is unstretched or stretched. The volume fraction of δ' phase, however, is significantly reduced in the stretched condition. The stretching treatment greatly accelerates the nucleation kinetics of T_1 phase at the expense of S' phase; however, the growth rate of T_1 phase (and also of S' phase) is significantly reduced in the stretched condition due to overlapping of the diffusion field. A kinetic model is presented that addresses this problem. The model successfully predicts the effect of stretching on the lengthening rate of T_1 plates. The activation energies for the lengthening of T_1 plates and S' rods are ~100 to 110 kJ/mole and ~110 to 120 kJ/mole, respectively, regardless of the condition of stretch. It is concluded that, for both unstretched and stretched material, the growth of the T_1 and S' phases is controlled by the diffusion of copper along dislocations. The nucleation of S' phase tends to occur at dislocations with a Burgers vector that is nearly parallel to the $[010]_{S'}$ direction, which is the direction that exhibits maximum misfit.

I. INTRODUCTION

Al-Li-Cu-Mg alloys are of great commercial interest because they offer high stiffness and lightness. The principal strengthening agents in ternary Al-Li-Cu alloys are the δ' (Al_3Li) and T_1 (Al_2CuLi) phases, particularly in the stretched condition.[1,2] The addition of magnesium is advantageous from a density standpoint and offers the possibility of utilizing additional precipitation of S' (Al_2CuMg) phase.

The δ' phase has an ordered $L1_2$ structure. T_1 phase has a hexagonal crystal structure (a = 0.497 nm, c = 0.935 nm), with an orientation relationship with the matrix of[3]

$$(0001)_{T_1} \parallel (111)_{Al}; \qquad [10\bar{1}0]_{T_1} \parallel [\bar{1}10]_{Al}$$

S' phase in Al-Li-Cu-Mg alloys has an orthorhombic crystal structure, with a = 0.404 nm, b = 0.925 nm, and c = 0.718 nm. The growth direction of S' lath is $[100]_{S'}$, and it has the following orientation relationship:[4]

$$[100]_{S'} \parallel [100]_{Al}; \qquad [010]_{S'} \parallel [021]_{Al};$$
$$[001]_{S'} \parallel [01\bar{2}]_{Al}$$

The equilibrium S phase in ternary Al-Cu-Mg alloys has the same crystal structure and orientation relationship, but slightly different lattice parameters.[4] It is difficult to distinguish between S' and S in Al-Li-Cu-Mg alloys, and no distinction has been attempted in this article.

The T_1 phase is an equilibrium phase and is known to nucleate heterogeneously in Al-Li-Cu alloys within the composition range of commercial interest, probably *via* a stacking fault mechanism[5] or *via* the dissociation of perfect dislocations in the vicinity of jogs.[6] Stretching is known to accelerate greatly the nucleation kinetics of T_1 phase,[7] probably through the promotion of dense areas of dislocation jogs.

The S' precipitation is also known to occur primarily by heterogeneous nucleation in alloys of medium magnesium content (~0.7 wt pct) and low copper content (~1.2 wt pct) (a typical composition of 8090 Al-Li alloy).[8] The stretching treatment encourages heterogeneous precipitation of fine S' particles at the expense of T_1 phase.[9,10,11] Homogeneous precipitation of S' phase is promoted in alloys of either high magnesium content (~1.0 wt pct) or medium copper content (~2.0 wt pct).[12,13] However, a predominant precipitation of T_1 phase is observed in low-magnesium (~0.5 wt pct) alloys.[10] The high-copper (~2.5 wt pct) alloys that contain a significant amount of magnesium (>~0.5 wt pct) have received comparatively little attention: increasing the copper content tends to promote θ' (Al_2Cu) and T_1 precipitation in place of S' precipitation. The stretching treatment suppresses θ' precipitation in favor of T_1 precipitation. The high magnesium content (>~1 wt pct) tends to promote S' precipitation. However, this case can lead to the precipitation of T_2 (Al_6CuLi_3) phase, particularly in alloys with very high copper contents (>~3 wt pct).[14,15] T_2 phase exerts little hardening effect. Stretching alters the precipitation kinetics of both the T_1 and S' phases in these high-copper alloys and can significantly affect the balance of the two phases. However, no detailed investigation of this effect has been reported. Furthermore, most previous investigations of precipitation in Al-Li-Cu-Mg alloys have been strictly qualitative. Only a few studies have focused on detailed precipitation kinetics, particularly of T_1 and S' phases.

J.-D. KIM, Graduate Student, and J.K. PARK, Professor, are with the Department of Materials Science and Engineering, Korea Advanced Institute of Science and Technology, 373-1, GusungDong, YusungGu, Taejon 305-701, Korea.

Manuscript submitted December 30, 1992.

The present investigation was undertaken to measure quantitatively the precipitation kinetics of δ', T_1, and S′ phases in an Al-2.0Li-2.8Cu-0.5Mg (wt pct) alloy and to evaluate the effect of stretching on the precipitation kinetics of the three phases.

II. EXPERIMENTS

The alloy, with a composition of Al-2.02Li-2.78Cu-0.48Mg-0.13Zr (wt pct), was cast in a vacuum induction furnace under an argon atmosphere using high-purity metals. It was homogenized, then hot- and cold-rolled to 2-mm-thick sheet. Samples were solution-treated at 530 °C for 30 minutes, quenched, and subsequently aged at elevated temperatures in either a silicon-oil bath or a salt bath controlled to ±1 °C. The aging behavior was measured using a Vickers hardness tester. Thin-foil specimens for transmission electron microscopy (TEM) were prepared by electrolytic polishing in a solution of 30 pct HNO_3 and 70 pct CH_3OH at ~−20 °C. The TEM observations were made at 200 keV using a PHILIPS CM20* microscope outfitted with scanning transmission electron microscopy (STEM) equipment. The foil thickness was measured using the contamination spot technique.

*PHILIPS CM20 is a trademark of Philips Electronic Instruments Corporation, Mahwah, NJ.

Correction for the effect of particle overlapping and truncation[16] was applied for the δ' volume fraction measurement in the underaged condition. In the overaged condition, only the truncation effect was taken into account. No correction for truncation was applied to the measurement of δ' particle sizes, because they were very small in comparison to the foil thickness. Maximum sizes of T_1 plates and S′ rods were measured to investigate their growth kinetics. In this case, no correction for truncation was required if the particles inclined with respect to the foil surface were embedded within the foil. The edge-on variants were actually used to measure the T_1 plate sizes. There are four variants in the T_1 phase, and it was assumed that all had equal populations. There are three types of S′ rods, corresponding to the three $\langle 100 \rangle_{Al}$ growth directions. In the unstretched condition, the population of each type was observed to be approximately the same size. However, only one type of rod was frequently observed in material in the stretched condition. The populations of T_1 and S′ phases differed from location to location. To minimize error, measurements were performed on several different grains.

III. RESULTS

Hardness measurements indicated that stretching significantly increases alloy hardness during the early stage of aging (Figure 1). This increase can be attributed not only to the strain hardening effect but also to an acceleration of aging kinetics brought on by the stretch treatment.

The microstructure of the alloy studied is complex because of the simultaneous presence of S′ and T_1 phases, in addition to δ' phase. The S′ phase has 12 variants,

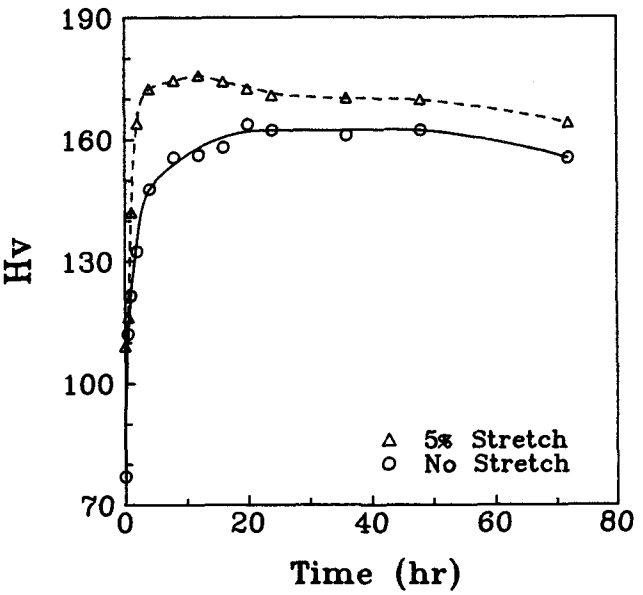

Fig. 1—Variation of Vickers hardness as a function of aging time at 190 °C.

four of which belong to the same growth direction, *i.e.*, $\langle 100 \rangle_{Al}$. The T_1 phase has four {111} variants. To help characterize the microstructure, a mixed diffraction pattern containing all the variants of the S′ and T_1 phases must be constructed. Figure 2 illustrates an example of the procedure in the presence of S′ phase. Figure 2(a) represents a mixed stereogram showing one of 12 S′ variants: $[100]_{S'} \parallel [100]_{Al}$; $[010]_{S'} \parallel [012]_{Al}$; $[001]_{S'} \parallel [0\bar{2}1]_{Al}$. The zone axis [110] of S′ phase becomes parallel (within 0.51 deg) to the [112] matrix zone axis. This is rotated to bring the [112] matrix zone axis to the projection center (Figure 2(b)). The mixed diffraction pattern for this variant is then constructed (Figure 2(c)). The structure factors for S′ phase are calculated using the atomic structure proposed by Mondolfo.[17] Figure 3 summarizes the result of the complete construction, including all the S′ phase variants.

A similar approach has been employed to construct the mixed diffraction pattern in the presence of T_1 phase. The result (Figure 4) is consistent with a previous report.[18] Figure 5 illustrates a final mixed diffraction pattern that includes S′, T_1, and δ' phases. An example of the observed diffraction pattern is shown in Figure 5(b), which is consistent with the calculated pattern in Figure 5(a), except for the presence of streaks. Four streaks are visible in Figure 5(b)—along $[11\bar{1}]$, $[\bar{2}01]$, $[02\bar{1}]$, and $[1\bar{1}0]$. The streak along $[11\bar{1}]$ is due to the edge-on T_1 plates on the $(11\bar{1})$ plane. The other streaks are due to three S′ laths grown along [010], [100], and [001] in the matrix. The S′ laths grown along [010] and [100] are gradually inclined with respect to the foil surface, whereas the one grown along [001] is steeply inclined.

Figure 6 illustrates δ' dark-field (DF) images in various conditions of stretch. Homogeneous nucleation is evident in all cases. Several θ' plates coated by δ' phase at low temperature are visible in the unstretched condition (Figure 6(a)). Stretching, however, tends to suppress θ' plates (Figure 6(b)). No θ' plates are observed

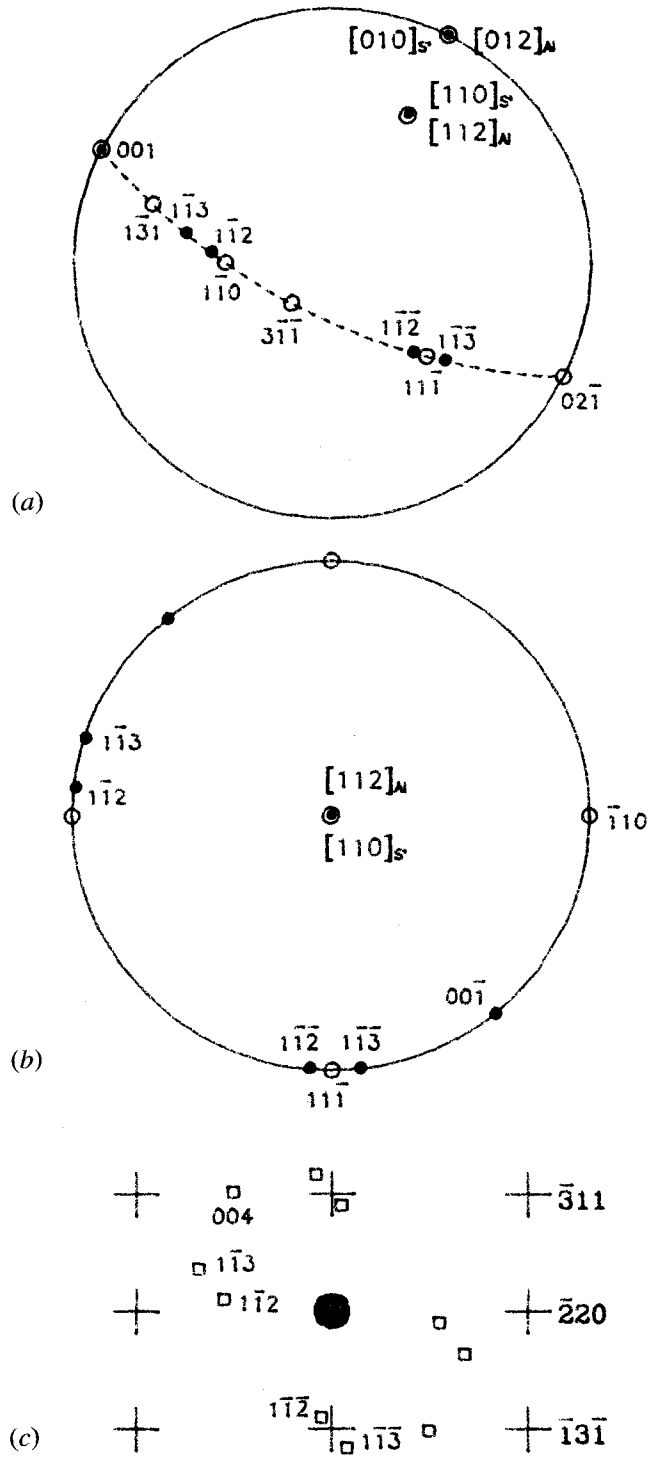

Fig. 2—Procedure for constructing a mixed diffraction pattern including S′ phase: (*a*) mixed stereogram showing the orientation relationship $[100]_{S'} \parallel [100]_{Al}$; $[010]_{S'} \parallel [012]_{Al}$; (*b*) mixed stereogram resulting from rotation of the zone axis $[112]_{Al}$ to the projection center; and (*c*) mixed diffraction pattern corresponding to the $[112]_{Al}$ zone axis.

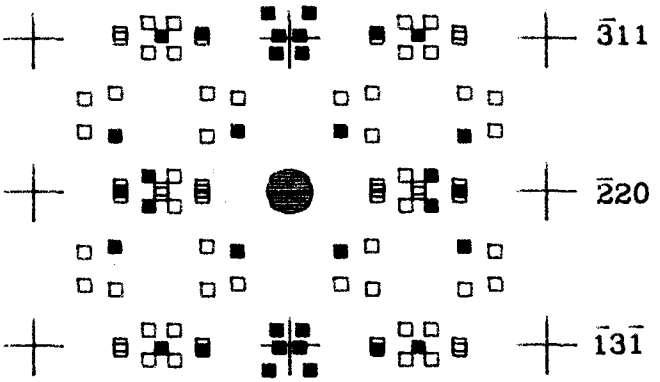

Fig. 3—Mixed diffraction pattern of $z = [112]_{Al}$ in the presence of S′ phase: +, reflections from the matrix; ■, reflections from the S′ phase; □, reflections arising from the double diffraction effect.

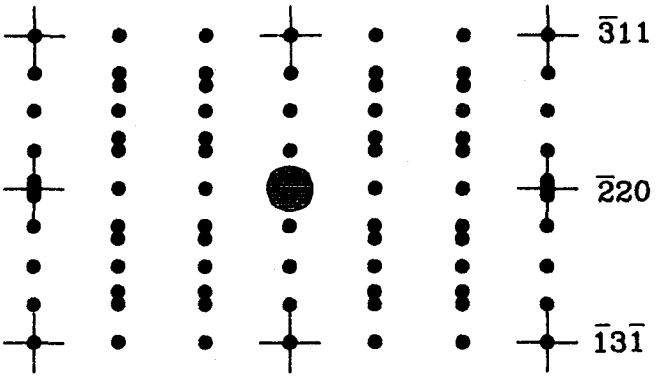

Fig. 4—Mixed diffraction pattern of $z = [112]_{Al}$ in the presence of T_1 phase: +, reflections from the matrix; ●, reflections from the T_1 phase. Includes the effect of extension of reciprocal lattice points due to the thinness of T_1 plates.

when the alloy is aged at temperatures above ~175 °C (Figure 6(c)).

The δ′ particle sizes have been measured using DF images such as those shown in Figure 6. It was shown[19] that the δ′ coarsening kinetics are best described by modified Lifshitz-Slyozov-Wagner theory,[20] apart from the particle distribution function. The theory predicts that

$$r^3 - r_0^3 = K(\phi) \cdot t$$

and

$$K(\phi) = \left(\frac{8\gamma C_e D V_m^2}{9RT}\right)\left(\frac{\rho(\phi)}{\rho(0)}\right) \qquad [1]$$

where ϕ is the volume fraction, γ is the interfacial energy, C_e is the equilibrium concentration, D is the lithium diffusivity, and $\rho(\phi)$ is the volume-fraction-dependent function. The cube of particle size plotted against aging time (Figure 7) shows a good linear relationship from the early stage of aging, suggesting an early start of the coarsening stage in agreement with previous reports.[21,22,23] Note, in particular, that stretching treatment has no significant influence on the δ′ coarsening kinetics. Measurement of particle sizes showed them to be similar in both conditions.

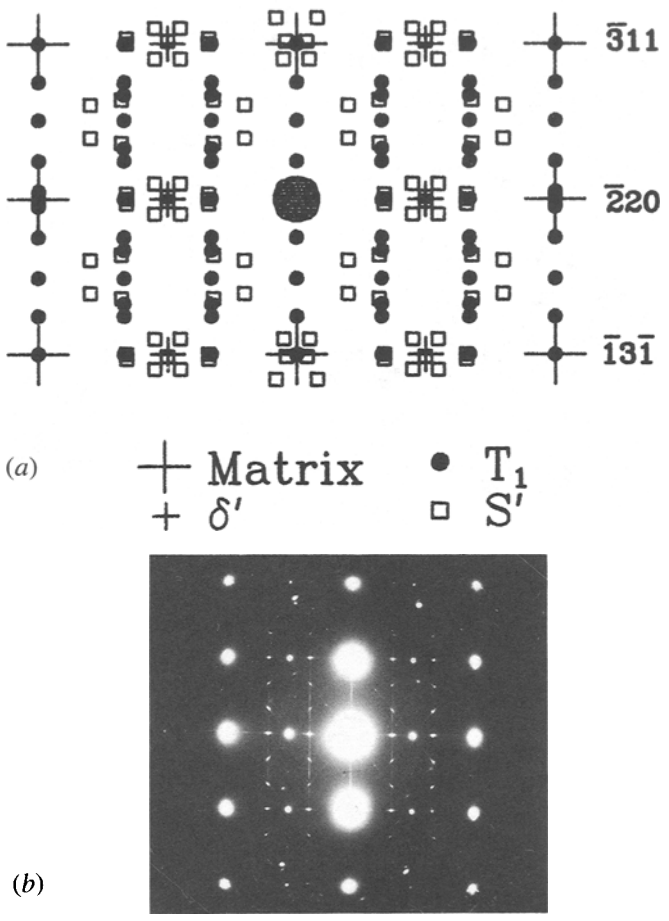

Fig. 5—Mixed diffraction pattern of $z = [112]_{Al}$ including S′, T_1, and δ′ phases: (*a*) constructed pattern; (*b*) observed selected-area diffraction pattern (SADP). Note in (b) the presence of a streak along $[11\bar{1}]$ due to T_1 phase and streaks along three directions—$[0\bar{2}1]$, $[\bar{2}01]$, and $[\bar{1}10]$—due to S′ phase.

The results of δ′ volume fraction measurements (Table I) indicate a nearly constant value (~2.7 pct) from the early stage of aging at temperatures near 175 °C, confirming the early onset of a coarsening stage. The volume fraction tends to decrease at a later stage, particularly at high temperature (~190 °C). This can probably be attributed to the increasing precipitation of T_1 phase and possibly also of δ phase. Results further show that stretching reduces the δ′ volume fraction by ~10 pct. This is due to an increase in the volume fraction of T_1 phase.

Equation [1] can be rearranged to give

$$\ln\left(\frac{K(\phi)\cdot T}{C_e}\right) = \ln\left(\frac{8\gamma D_0 V_m^2 \rho(\phi)}{9R\rho(0)}\right) + \left(\frac{-Q}{RT}\right) \quad [2]$$

where Q is the activation energy for lithium diffusion. Figure 8 shows the plot $\ln (K(\phi)\cdot T/C_e)$ *vs* $1/T$. The activation energies can be estimated from the slope: 102.9 kJ/mole and 105.8 kJ/mole in the unstretched and stretched conditions, respectively. These energies are somewhat lower than those in an Al-Li-Cu ternary alloy (~120 to 130 kJ/mole)[24,25] and in Al-Li binary alloys (~120 to 140 kJ/mole).[22,26,27,28]

Figure 9 illustrates examples of S′ and T_1 phases in the unstretched and stretched conditions. Both cases contain S′ and T_1 phases. The proportion of each phase changes drastically as a result of stretching. In the unstretched condition (Figure 9(b)), there are significant amounts of edge-on T_1 plates and of S′ rods grown along [010] (projection direction: $[\bar{1}5\bar{2}]$). In the stretched condition (Figure 9(d)), T_1 plates become much finer and more numerous, whereas S′ rods tend to be finer but scarce. This indicates that stretching promotes the T_1 nucleation rate at the expense of S′ precipitation—an observation that is in direct contradiction with previous reports regarding low-copper quaternary alloys.[9] The discrepancy probably arises from the dependence of the relative stability of the two phases on the copper-magnesium ratio.

Examination of SADPs indicates, in the unstretched condition (Figure 9(a)), the presence of three streaks (along $[0\bar{2}1]$, $[\bar{2}01]$, and $[\bar{1}10]$) due to S′ rods grown along three $\langle 100\rangle_{Al}$ directions. However, in the stretched condition (Figure 9(c)), only one streak appears along $[\bar{2}01]$, which is due to rods grown along $[010]_{Al}$. Numerous observations frequently have indicated that S′ rods grow along only one of three $\langle 100\rangle_{Al}$ directions, the other two being nearly absent. This is in clear contrast to the unstretched case, where the rods grown along three $\langle 100\rangle$ directions have nearly equal populations.

The volume fraction of T_1 plates has been measured (Table I) using DF images such as those shown in Figure 9. The volume fraction gradually increases with aging time, which suggests that T_1 precipitation and δ′ precipitation have different growth stages. Stretching abruptly increases the T_1 volume fraction—*e.g.*, from ~2 pct to ~4 pct at 175 °C. This effect is less pronounced at a high temperature of 190 °C. At this temperature, the volume fraction tends to increase rapidly even in the unstretched condition, probably because of a high diffusion rate.

The sizes of T_1 plates and S′ rods have been measured using DF images. According to the Zener-Hillert theory,[29] the lengthening rate of solute-rich plate edges (of β phase) is linear as long as the radius of curvature, r, remains constant:

$$\frac{dL}{dt} = \frac{D(C_0 - C_\alpha^{\alpha\beta})}{2kr(C_\beta^{\beta\alpha} - C_\alpha^{\alpha\beta})} \quad [3]$$

where C_0 is the initial alloy composition, $C_\alpha^{\alpha\beta}$ is the equilibrium composition in the matrix with respect to the β (T_1) phase, $C_\beta^{\beta\alpha}$ is the equilibrium composition of β phase, and k is a constant. Figure 10 plots the maximum plate diameter *vs* aging time. The stretched condition exhibits a much slower growth rate, an observation in agreement with a previous report on an Al-Li-Cu ternary alloy.[7] Because the volume fraction is large in the stretched condition, the number density per unit volume, Nv, is expected to be larger in this condition as well. Measurement indicated that Nv is promoted by an order of magnitude, *i.e.*, from $\sim 10^2/\mu m^3$ in the unstretched condition to $\sim 10^3/\mu m^3$ in the stretched condition (near peak aging condition at 175 °C). Figure 10 indicates a

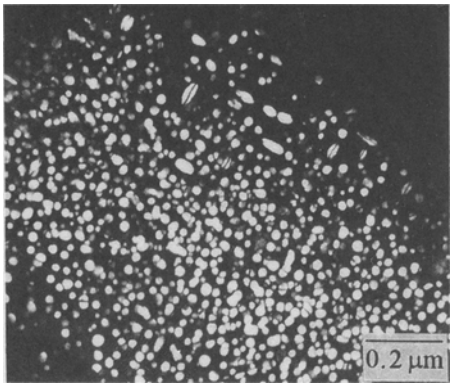

(*a*)

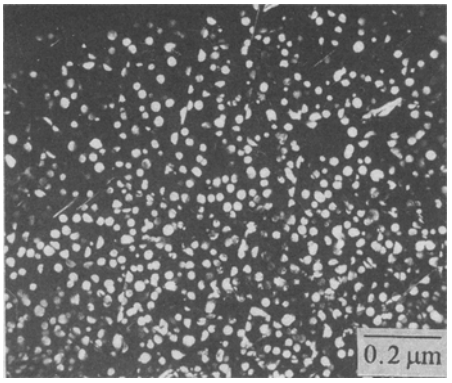

(*b*)

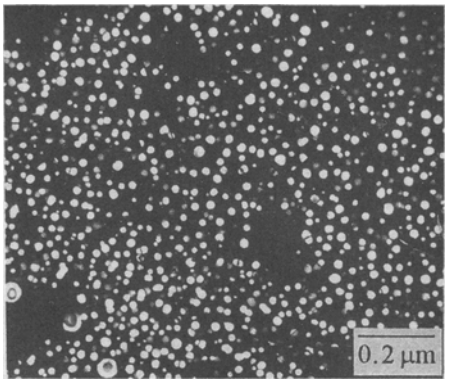

(*c*)

Fig. 6—Dark-field images taken using superlattice reflection due to δ' phase: (*a*) sample aged at 160 °C for 96 h in the unstretched condition; (*b*) sample aged at 160 °C for 96 h in the 5 pct stretch condition; and (*c*) sample aged at 190 °C for 8 h in the unstretched condition.

significant deviation from the linear growth rate expected from Eq. [3]. This discrepancy is more pronounced in the stretched condition, suggesting that it is primarily due to the effect of overlapping diffusion field.

In an attempt to solve this problem, C_0 in Eq. [3] has been replaced with time-dependent $C_0(t)$ as a first approximation, *i.e.*,

$$\frac{dL}{dt} = \frac{D(C_0(t) - C_\alpha^{\alpha\beta})}{2kr(C_\beta^{\beta\alpha} - C_\alpha^{\alpha\beta})} \qquad [4]$$

It was further assumed that the supersaturation, $C_0(t) - C_\alpha^{\alpha\beta}$, varies sinusoidally with distance, as in the case of ingot homogenization.[30] The supersaturation at the center of the diffusion field becomes

$$C_0(t) - C_\alpha^{\alpha\beta} = (C_0 - C_\alpha^{\alpha\beta}) \exp\left(\frac{-\pi^2 Dt}{\lambda^2}\right) \qquad [5]$$

where λ is a linear measure of the diffusion field length. Note that Eq. [5] differs only slightly from the first-term approximation of the complete solution of diffusion equation at the boundary conditions, which are similar to those in the decarburization problem.[31] Equation [4] is then

$$\frac{dL}{dt} = K_1 \cdot D \cdot \exp\left(\frac{-\pi^2 Dt}{\lambda^2}\right) \qquad [6]$$

where

$$K_1 = \frac{C_0 - C_\alpha^{\alpha\beta}}{2kr(C_\beta^{\beta\alpha} - C_\alpha^{\alpha\beta})}$$

Integration gives

$$L = K_0\left[1 - \exp\left(\frac{-\pi^2 Dt}{\lambda^2}\right)\right] \qquad [7]$$

where

$$K_0 = K_1 \cdot \frac{\lambda^2}{\pi^2}$$

If the exponent in Eq. [6] is small ($<\sim 0.5$),

$$\frac{dL}{dt} \cong K_1 \cdot D\left(1 - \frac{\pi^2 Dt}{\lambda^2}\right) \qquad [8]$$

Integration yields

$$\frac{L}{t} = K_1 \cdot D - K_2 \cdot D^2 \cdot t \qquad [9]$$

where

$$K_2 = K_1 \cdot \frac{\pi^2}{2\lambda^2}$$

Equation 9 predicts a linear decrease of L/t with t. The negative slope of the line is proportional to the square of the diffusion coefficient, and the intercept is directly proportional to the diffusivity. Figure 11 replots the data according to Eq. [9]. The result shows that a linear relationship is satisfied during the initial stage at high temperatures and that it extends to a longer time at low temperatures. The logarithms of the slopes and of the intercepts are plotted as a function of the inverse of absolute temperature in Figure 12. Analysis of the intercepts yields activation energies of 107.4 kJ/mole and 111.6 kJ/mole in the unstretched and stretched conditions, respectively. The corresponding activation energies from the slopes are 104.0 kJ/mole and 110.9 kJ/mole, respectively. The two results are in good agreement, which partly justifies the present model. There is no significant difference in activation energy

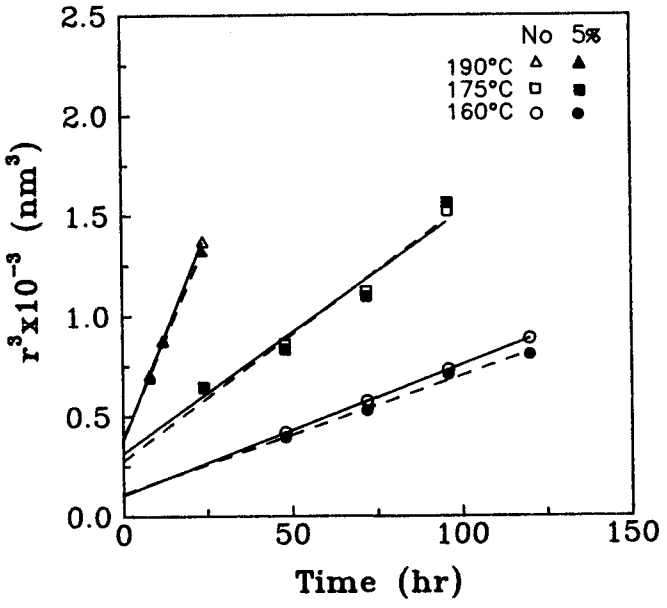

Fig. 7—Variation of the cubes of δ' particle radii as a function of aging time at various temperatures, depending on the condition of stretch.

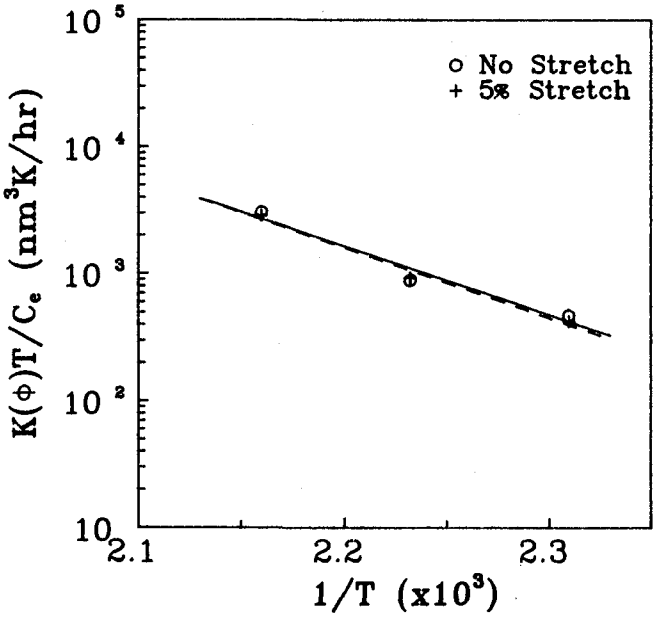

Fig. 8—Arrhenius plot of the coarsening rate of δ' particles in both the unstretched and stretched conditions.

regardless of the condition of stretch, which suggests that the diffusion mechanism is the same in both conditions.

Figure 13 shows a similar plot for the case of S′ rods in the unstretched condition. The activation energies are 113.3 kJ/mole and 123.1 kJ/mole from the intercepts and from the slopes, respectively. Measurement indicated that the number density in the stretched condition decreases to only ~10 pct of that of the unstretched condition. This is due to an acceleration of T_1 precipitation in the stretched condition. It was difficult to test the stretching effect because of the scarcity of S′ rods.

IV. DISCUSSION

The activation energy for δ' coarsening is estimated to be ~100 kJ/mole, regardless of the condition of stretch. This value is somewhat lower than that reported for an Al-Li-Cu ternary alloy (~120 to 130 kJ/mole)[24,25] and for Al-Li binary alloys (~120 to 140 kJ/mole).[22,26,27,28] This could simply be due to the difference in the δ' volume fraction. However, the present results appear to indicate that activation energy is nearly independent of the condition of stretch, although the δ' volume fraction is decreased by ~10 pct in the stretched condition. Furthermore, the principal microstructural constituents in the stretched condition are similar to those in Al-Li-Cu ternary alloys, except for the presence of a minor amount of S′ phase. This leads us to conclude that there is a small difference in the activation energy between the quaternary and ternary alloys and that the difference is due to the presence of magnesium. Magnesium is reported to be incorporated into δ' particles,[32] although its precise role is unknown at the present time.

The intercept K_1D in Eq. [9] is the coefficient of the linear growth rate of the original Zener-Hillert equation, which represents the situation in the absence of the problem of overlapping diffusion field. The effect of overlapping diffusion field is incorporated in the slope of the plot K_2D^2. Thus, Eq. [9] predicts the same intercept regardless of the condition of stretch. At the same time, it predicts a steeper slope when the alloy is stretched, because the interparticle distance λ is expected to decrease as a result of stretching.

Results for T_1 plates (Figure 11) indicate that taking

Table I. Volume Fraction of δ' and T_1 Phases in Various Aging Conditions

Aging Condition	δ' Phase		T_1 Phase	
	Unstretched	5 Pct Stretch	Unstretched	5 Pct Stretch
175 °C				
24 hours	0.028	0.025	0.010	0.022
48 hours	0.027	0.024	0.014	0.032
72 hours	0.025	0.023	0.022	0.040
190 °C				
8 hours	0.028	0.023	0.008	0.016
12 hours	0.025	0.022	0.015	0.027
24 hours	0.023	0.022	0.022	0.032

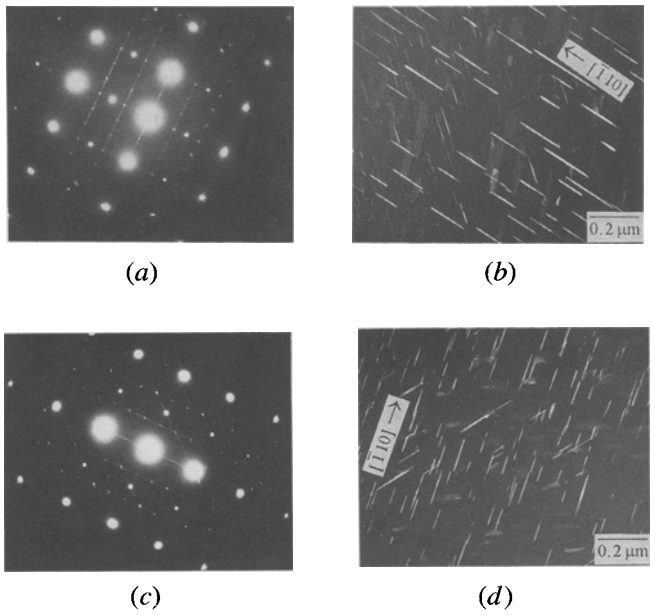

Fig. 9—Selected-area diffraction patterns of the zone axis near $[112]_{Al}$ and DF images taken using reflections including both the T_1 and S′ phases in a sample aged at 160 °C for 96 h: (*a*) SADP in the unstretched condition; (*b*) DF image in the unstretched condition; (*c*) SADP in the stretched condition; (*d*) DF image in the stretched condition. Particles seen along $[\bar{1}10]_{Al}$ are edge-on T_1 plates and particles seen along $[\bar{1}5\bar{2}]_{Al}$ are S′ rods. Note the presence of streaks due to S′ rods along all three directions (*i.e.*, $[0\bar{2}1]$, $[\bar{2}01]$, and $[\bar{1}10]$) in (a), but of a streak along only one direction ($[\bar{2}01]$) in (c).

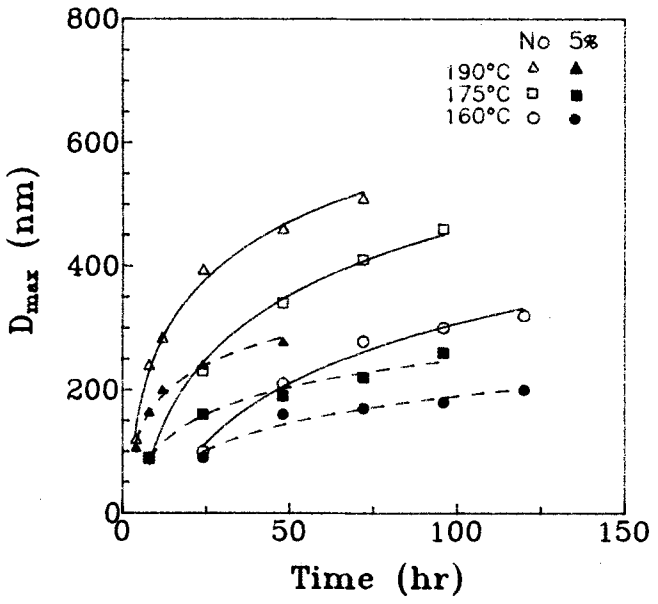

Fig. 10—Variation of maximum plate diameter (D_{max}) of T_1 phase as a function of aging time at various temperatures, depending on the condition of stretch. The lengthening rate of T_1 plates is significantly reduced in the stretched condition.

the data during the initial stage of aging leads to similar intercepts under the two different conditions, in agreement with the prediction. It is also evident that the initial slope of the data in the stretched condition is somewhat larger than that in the unstretched condition, *i.e.*, by

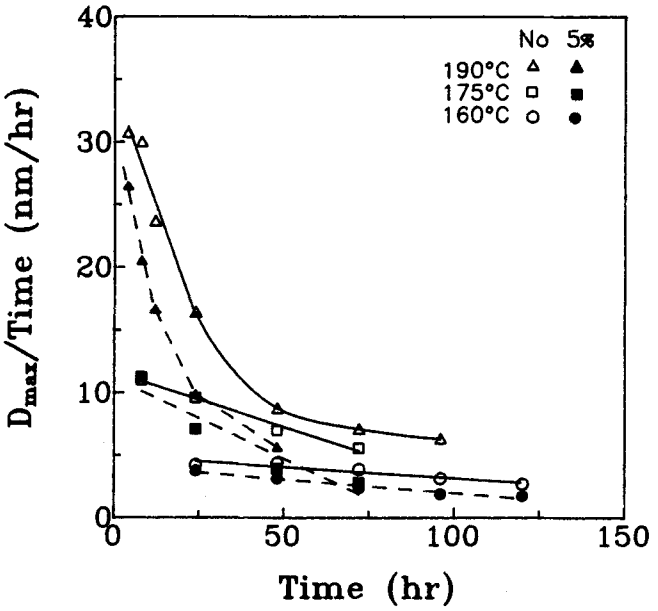

Fig. 11—Variation of D_{max}/time of T_1 phase as a function of aging time according to Eq. [9] at various temperatures, depending on the condition of stretch. A significant deviation from linearity occurs at a later stage of aging at 190 °C.

~1.5 times for all temperatures. The condition for the approximation within ~10 pct error in Eq. [9] is $\pi^2 Dt/\lambda^2 < 0.5$. An estimation using $\lambda \sim 120$ nm indicates that the condition holds at times of less than ~20 hours at ~190 °C. Thus, the use of data obtained during the initial stage of aging is a necessary condition at comparatively high temperatures. Examination of the T_1 dispersion indicated that λ is typically ~120 nm and ~85 nm in the unstretched and stretched conditions, respectively. The ratio of the slope in Eq. [9] is thus predicted to be ~2.0, which is in reasonable agreement with the observed ratio. These results strongly support the contention that the present model can be used as a reasonable approximation for treating the problem of overlapping diffusion field.

The activation energies for the growth of T_1 plates are estimated to be in the range of ~100 to 110 kJ/mole, regardless of the condition of stretch, suggesting that the growth of T_1 plates occurs by the same diffusion mechanism in both the unstretched and stretched conditions. Comparison with the literature indicates that the activation energy is very close to that reported for the case of grain-boundary diffusion of copper in aluminum[33] (~105 kJ/mole). The activation energy for the growth of S′ rods in the unstretched condition is estimated to be a similar value (~110 to 120 kJ/mole). This leads us to conclude that the growth of both T_1 and S′ phases is controlled by the diffusion of copper through dislocations. The activation energy along a dislocation is expected to be similar to that along a grain boundary.

The present model has several deficiencies, however. The first is the exaggeration of the linear gradient approximation for the diffusion field. The second is the lack of consideration of the effect of decreasing λ with time due to plate lengthening. Fortunately, the first approximation generally leads to a slower growth rate,[34]

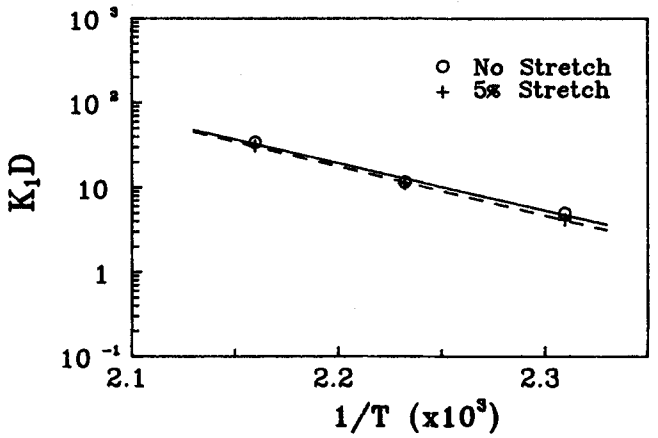

(*a*)

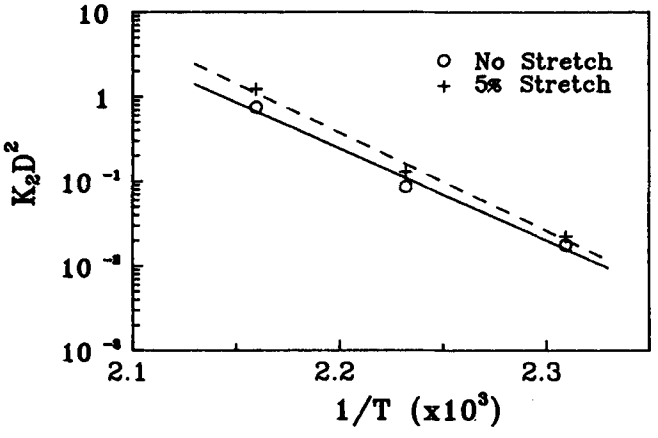

(*b*)

Fig. 12—Arrhenius plots of (*a*) the intercepts and (*b*) the slopes using the data in Figure 11 obtained during the early stage of aging. Note the close correspondence of the two intercepts depending on the condition of stretch in (a).

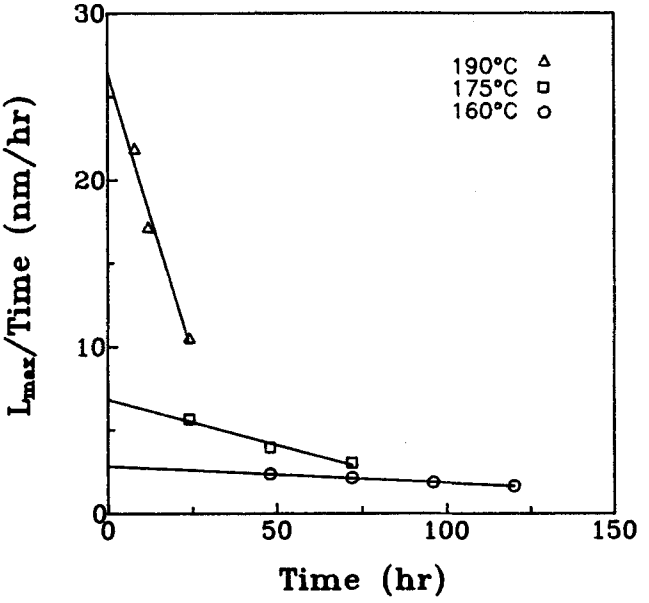

Fig. 13—Variation of D_{max}/time of S′ phase as a function of aging time according to Eq. [9] at various temperatures in the unstretched condition.

whereas the second leads to a faster growth rate. The model also oversimplifies the concentration profile during initial aging time. This treatment is therefore more appropriate in a situation where the overlapping of diffusion field begins to occur.

The stretching treatment tends to facilitate the growth of S′ rods in only one of three possible $\langle 100 \rangle_{Al}$ directions, probably due to the strain energy effect on S′ nucleation. The misfit parameters of the S′ phase differ depending on the three principal crystal axes;[35] the maximum misfit occurs along the **b** crystal axis. One would then expect a maximum release of strain energy when the S′ phase nucleates on dislocations with a Burgers vector that is parallel to its **b** axis. Examination of the orientation relationship indicates that if the Burgers vector is parallel to [110], for example, only one growth direction (*i.e.*, $[001]_{Al}$) can make the **b** axis of S′ phase nearly parallel (~18.4 deg) to the given Burgers vector. This is true only for the two of four variants that belong to this growth direction. Those S′ precipitates grown along the other directions (*i.e.*, $[010]_{Al}$ and $[001]_{Al}$) always make the angle larger than 50.8 deg. This thus explains why the S′ rods grow in only one of three $\langle 100 \rangle_{Al}$ directions in the stretched condition, if one assumes that the dislocations controlling the plastic flow have the same Burgers vector in a given grain. It is in fact reported that these dislocations are predominantly screw type in this alloy system.[36] Thus, it is quite possible that these parallel dislocations have the same Burgers vector. In the unstretched condition, the types of dislocations or their Burgers vectors are not necessarily the same. One can therefore anticipate equal populations of S′ phase in the three $\langle 100 \rangle$ growth directions.

V. CONCLUSIONS

The microstructure of an Al-2.0Li-2.8Cu-0.5Mg (-0.13Zr) alloy consists primarily of δ', S′, and T_1 phases. Stretching exerts little influence on the coarsening kinetics of the δ' particles. The activation energy for δ' coarsening is estimated to be ~100 kJ/mole, regardless of the condition of stretch, which is somewhat lower than that in an Al-Li-Cu ternary alloy. The volume fraction of δ' phase, however, is significantly reduced (by ~10 pct) in the stretched condition. The stretching treatment greatly accelerates the nucleation kinetics of T_1 phase at the expense of S′ phase; however, the growth rate of T_1 phase (and also of S′ phase) is significantly reduced in the stretched condition due to the effect of overlapping diffusion field. A model has been presented to accommodate this problem. The effect of stretching on the lengthening rate of T_1 plates can be successfully predicted. The activation energy for the lengthening of T_1 plate is estimated to be ~100 to 110 kJ/mole, regardless of whether the alloy is unstretched or stretched. A similar activation energy value (~110 to 120 kJ/mole) is observed for the growth of S′ rods. It is concluded that the growth of both T_1 and S′ phases in

any condition of stretch is controlled by the diffusion of copper along dislocations. The nucleation of S′ phase is greatly influenced by misfit strain energy and tends to occur at dislocations with a Burgers vector that is nearly parallel to the $[010]_{S'}$ direction, which is the direction that exhibits maximum misfit.

ACKNOWLEDGMENT

The authors are grateful to the Agency for Defense Development and to the Ministry of Science and Technology for their financial support of this research.

REFERENCES

1. J.C. Huang and A.J. Ardell: *Acta Metall.*, 1988, vol. 36, pp. 2995-3006.
2. W.A. Cassada, G.J. Shiflet, and E.A. Starke, Jr.: *4th Int. Aluminium Lithium Conf.*, G. Champier, B. Dubost, D. Miannay, and L. Sabetay, eds., *J. Phys.*, Les Ulis, France, 1987, Colloque C3, pp. 397-406.
3. H.K. Hardy and J.M. Silcock: *J. Inst. Met.*, 1955–1956, vol. 84, pp. 423-28.
4. G.W. Lorimer: *Precipitation Process in Solids*, K.C. Russell and H.J. Aaronson, eds., TMS-AIME, Warrendale, PA, 1978, p. 106.
5. B. Noble and G.E. Thompson: *Met. Sci. J.*, 1972, vol. 6, pp. 167-74.
6. W.A. Cassada, G.J. Shiflet, and E.A. Starke, Jr.: *Metall. Trans. A*, 1991, vol. 22A, pp. 287-97.
7. W.A. Cassada, G.J. Shiflet, and E.A. Starke, Jr.: *Metall. Trans. A*, 1991, vol. 22A, pp. 299-306.
8. H.M. Flower and P.J. Gregson: *Mater. Sci. Technol.*, 1987, vol. 3, pp. 81-90.
9. P.J. Gregson and H.M. Flower: *Acta Metall.*, 1985, vol. 33, pp. 527-37.
10. S.J. Harris, B. Noble, and K. Dinsdale: *4th Int. Aluminium Lithium Conf.*, G. Champier, B. Dubost, D. Miannay, and L. Sabetay, eds., *J. Phys.*, Les Ulis, France, 1987, Colloque C3, pp. 415-23.
11. K. Welpmann, M. Peters, and T.H. Sanders, Jr.: *Aluminium-Lithium Alloys III*, C. Baker, P.J. Gregson, S.J. Harris, and C.J. Peel, eds., The Institute of Metals, London, 1986, pp. 524-29.
12. P.J. Gregson, H.M. Flower, C.N.J. Tite, and A.K. Mukhopadhyay: *Mater. Sci. Technol.*, 1986, vol. 2, pp. 349-53.
13. P.J. Gregson, C.J. Peel, and B. Evans: *Aluminium-Lithium Alloys III*, C. Baker, P.J. Gregson, S.J. Harris, and C.J. Peel, eds., The Institute of Metals, London, 1986, pp. 516-23.
14. P. Sainfort and B. Dubost: *4th Int. Aluminum Lithium Conf.*, G. Champier, B. Dubost, D. Miannay, and L. Sabetay, eds., *J. Phys.*, Les Ulis, France, 1987, Colloque C3, pp. 407-13.
15. R.J. Kar, J.W. Bohlen, and G.R. Chanani: *Aluminium-Lithium Alloys II*, E.A. Starke, Jr. and T.H. Sanders, Jr., eds., TMS-AIME, Warrendale, PA, 1984, pp. 255-85.
16. E.E. Underwood: *Quantitative Stereology*, Addison-Wesley, Reading, MA, 1970, pp. 173-78.
17. L.F. Mondolfo: *Aluminum Alloys: Structure and Properties*, Butterworths, London, 1976, pp. 497-505.
18. J.C. Huang and A.J. Ardell: *Mater. Sci. Technol.*, 1987, vol. 3, pp. 176-88.
19. K. Mahalingan, B.P. Gu, G.L. Liedl, and T.H. Sanders, Jr.: *Acta Metall.*, 1987, vol. 35, pp. 483-98.
20. A.J. Ardell: *Acta Metall.*, 1972, vol. 20, pp. 61-71.
21. S.F. Baumann and D.B. Williams: *Scripta Metall.*, 1984, vol. 18, pp. 611-16.
22. D.B. Williams and J.W. Edington: *Met. Sci.*, 1975, vol. 9, pp. 529-32.
23. M. Ahmad and T. Ericsson: *Scripta Metall.*, 1985, vol. 19, pp. 457-62.
24. J.C. Huang and A.J. Ardell: *Aluminium-Lithium Alloys III*, C. Baker, P.J. Gregson, S.J. Harris, and C.J. Peel, eds., The Institute of Metals, London, 1986, pp. 455-70.
25. W.S. Jung and J.K. Park: *Scripta Metall.*, 1992, vol. 26, pp. 831-36.
26. S.C. Jha, T.H. Sanders, Jr., and M.A. Dayananda: *Acta Metall.*, 1987, vol. 35, pp. 473-82.
27. W.S. Jung and J.K. Park: *Aluminum-Lithium Alloys*, Materials and Component Engineering Publications Ltd., Birmingham, United Kingdom, 1989, pp. 595-604.
28. B. Noble and G.E. Thompson: *Met. Sci. J.*, 1971, vol. 5, pp. 114-20.
29. H.I. Aaronson, C. Laird, and K.R. Kinsman: *Phase Transformations*, ASM, Metals Park, OH, 1969, pp. 325-28.
30. P.G. Shewmon: *Transformations in Metals*, McGraw-Hill, New York, NY, 1969, pp. 41-43.
31. P.G. Shewmon: *Diffusion in Solids*, McGraw-Hill, New York, NY, 1963, pp. 16-19.
32. S.F. Baumann and D.B. Williams: *Aluminum-Lithium Alloys II*, E.A. Starke, Jr. and T.H. Sanders, Jr., eds., TMS-AIME, Warrendale, PA, 1984, pp. 17-29.
33. K. Przybylowicz: *Handbook of Grain and Interphase Boundary Diffusion Data*, I. Kaur, W. Gust, and L. Kozma, eds., Ziegler Press, Stuttgart, Germany, 1989, p. 125.
34. H.B. Aaron, D. Fainstein, and G.R. Kotler: *J. Appl. Phys.*, 1970, vol. 41, pp. 4404-10.
35. B.N. Wilson and P.G. Partridge: *Acta Metall.*, 1965, vol. 13, pp. 1321-27.
36. J.C. Huang and A.J. Ardell: *Mater. Sci. Eng.*, 1988, vol. A104, pp. 149-56.